Australian Meteorological and Oceanographic Journal 62 (2012) 179–192

Seasonal climate summary southern hemisphere (spring 2011): La Niña returns

D.A. Cottrill
Centre for Australian Weather and Climate Research (CAWCR),
Bureau of Meteorology, Australia

(Manuscript received August 2012; revised September 2012)

The southern hemisphere circulation patterns and associated anomalies for the austral spring 2011 are reviewed, with emphasis on the Pacific Basin climate indicators and Australian rainfall and temperature. Near neutral sea surface temperatures across the equatorial Pacific Ocean in winter began to cool in the spring, with the onset of La Niña conditions and below average subsurface temperatures. The Indian Ocean Dipole was positive, with cooler waters off the Indonesian coast but generally warmer than average temperatures over the Indian Ocean. Moderate positive values of the Southern Oscillation Index and negative values of the 5VAR index occurred, although not as strong as in spring 2010. Australia had much above average rainfall during spring 2011 (the ninth highest on record), especially in Western Australia, the Northern Territory and parts of South Australia, Queensland and New South Wales. Although below average rainfall fell in September over Australia, above average rainfall occurred in October and November, with every State receiving above average rainfall for November. Maximum and minimum temperatures were slightly above average over most of Australia, especially in Victoria, Tasmania, South Australia and New South Wales, and below average in the Northern Territory and Western Australia, where rainfall was higher.

Introduction

This summary reviews the southern hemisphere and equatorial climate patterns for spring 2011, with particular attention given to the Australasian and Pacific regions. The main sources of information for this report are analyses prepared by the Bureau of Meteorology's National Climate Centre (NCC) and the Centre for Australian Weather and Climate Research (CAWCR).

Pacific and Indian Basin climate indices

Southern Oscillation Index

Weak to moderate positive values of the Troup Southern Oscillation Index[1] (SOI) strengthened from winter 2011, and persisted through spring of 2011. Monthly SOI values were: +11.7 (September), +7.3 (October) and +13.8 (November), with an average spring SOI value of +10.9. The moderate positive values of the SOI indicated the early development of La Niña conditions in the Pacific Ocean, but considerably weaker than the near record SOI values for spring 2010 (Lovitt, 2011). Last year, the near record SOI values occurred prior to one of the strongest La Niña events on record, which produced Australia's second wettest summer (Imielska, 2011). Figure 1 shows the monthly SOI from January 2007 to November 2011, together with a five-month weighted moving average.

The spring MSLP values were generally average at Darwin but above the long-term average at Tahiti, indicating that the anomaly at Tahiti was mainly responsible for the positive values in the SOI. The monthly anomalies for September, October and November for Darwin were +0.6 hPa, -0.4 hPa and -0.2 hPa respectively and for Tahiti were +2.5 hPa, +0.9 hPa and +1.9 hPa respectively.

Composite monthly ENSO index (5VAR)

5VAR[2] is a composite monthly ENSO index, calculated as the standardised amplitude of the first principal component of

[1]The Troup Southern Oscillation Index (Troup 1965) used in this article is ten times the standardised monthly anomaly of the difference in mean sea-level pressure (MSLP) between Tahiti and Darwin. The calculation is based on a 60-year climatology (1933–92). The Darwin MSLP is provided by the Bureau of Meteorology, with the Tahiti MSLP being provided by Météo France interregional direction for French Polynesia.

Corresponding author address: D.A. Cottril, Bureau of Meteorology, GPO Box 1289, Melbourne 3001, Australia.
Email: a.cottrill@bom.gov.au

[2]ENSO 5VAR was developed at the Bureau's National Climate Centre and is described in Kuleshov et al. (2009). The principal component analysis and standardisation of this ENSO index is performed over the period 1950–99.

Fig. 1. Southern Oscillation Index, from January 2007 to November 2011, together with a five-month binomially weighted moving average. Means and standard deviations used in the computation of the SOI are based on the period 1933–92.

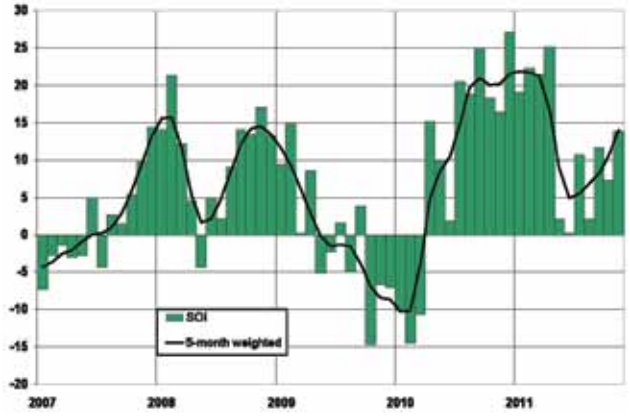

Fig. 2. 5VAR composite standardised monthly ENSO index from January 2007 to November 2011, together with a weighted three-month moving average. See text for details.

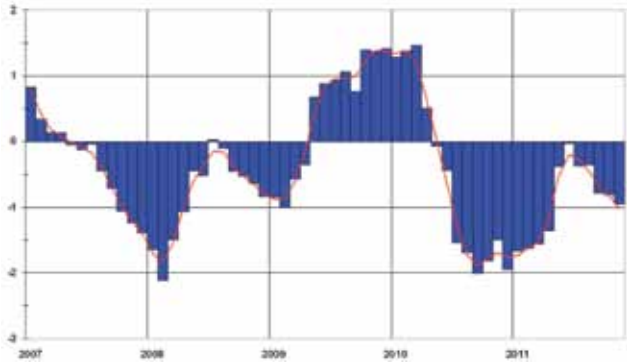

monthly Darwin and Tahiti mean sea-level pressure (MSLP)[3] and monthly NINO3, NINO3.4 and NINO4 sea surface temperatures[4] (SSTs). The sequence of monthly 5VAR values from January 2007 to November 2011, with a weighted three-month moving average is shown in Fig. 2. The 5VAR index was moderately negative during spring, a change from the near neutral 5VAR values during the preceding winter. The 5VAR value for the month of September was -0.78, followed by October (-0.81) and November (-0.95), with an average value for spring of -0.85. A decrease in the 5VAR values from winter indicates a cooling of the SSTs in the equatorial Pacific Ocean and the developing La Niña conditions.

The Multivariate ENSO Index[5] (MEI), produced by the US Climate Diagnostics Center, is derived from a number of atmospheric and oceanic parameters calculated as a two-month mean. Significant negative (positive) anomalies are typically associated with La Niña (El Niño) events. The MEI values for September–October and October–November were -0.97 and -0.98 respectively, not as low as the same period last year prior to the strong La Niña event. If the historical MEI values are ranked from 1950 to 2011, the two periods rank fourteenth and sixteenth lowest respectively for the bimonthly historical MEI values.

Outgoing long-wave radiation

Outgoing long-wave radiation (OLR) over the equatorial Pacific Ocean near the Date Line (5°S to 5°N and 160°E to 160°W) is a good proxy for tropical convection and rainfall. Positive (negative) OLR anomalies indicate suppressed (enhanced) convection and usually occur in La Niña (El Niño) years in this region. The Climate Prediction Center, Washington, computes a standardised monthly OLR anomaly[6] over the equatorial Pacific for the equatorial region ranging from 5°S to 5°N. The monthly OLR anomaly values for September, October and November were +0.3, +1.1 and +1.0 respectively. The seasonal average for spring was +0.8 and indicated convection was suppressed over this equatorial Pacific Ocean region during this time.

The spatial pattern of seasonal OLR anomalies across the Asia-Pacific tropics for spring 2011 is shown in Fig. 3. Consistent with the positive OLR anomalies discussed above, the tropical Pacific around the international dateline shows positive OLR values, indicating suppressed convection in the region northeast of the Solomon Islands and over the eastern Indian Ocean, southwest of Sumatra. In contrast, over parts of Indonesia, Papua New Guinea, much of Australia and the southwest Pacific, the OLR anomalies were negative, indicating increased convection and rainfall. This OLR pattern is consistent with the developing La Niña conditions over the equatorial Pacific Ocean.

Indian Ocean Dipole

The Indian Ocean Dipole (IOD) is the difference between the SSTs in the western (50°E to 70°E and 10°S to 10°N) and eastern (90°E to 110°E and 10°S to 0°S) equatorial Indian Ocean. The index is called the Dipole Mode Index (DMI) and was first described by Saji et al. (1999). A positive (negative) IOD is characterised by cooler (warmer) than normal water in the tropical eastern Indian Ocean and warmer (cooler) than normal water in the tropical western Indian Ocean. A positive IOD SST pattern has been shown to be associated with a decrease in rainfall over parts of central and southern Australia in austral winter and spring, whereas a negative IOD SST pattern is usually associated with higher rainfall.

[3]MSLP data obtained from http://www.bom.gov.au/climate/current/soihtm1.shtml. As previously mentioned, the Tahiti MSLP data are provided by Météo France inter-regional direction for French Polynesia.
[4]SST indices obtained from ftp://ftp.cpc.ncep.noaa.gov/wd52dg/data/indices/sstoi.indices.
[5]Multivariate ENSO Index obtained from http://www.esrl.noaa.gov/psd/people/klaus.wolter/MEI/table.html. The MEI is a standardised anomaly index described in Wolter and Timlin (1993, 1998).

[6]Obtained from http://www.cpc.ncep.noaa.gov/data/indices/olr.

Fig. 3. OLR anomalies for spring 2011 (W m^{-2}). Base period 1979–2000. The mapped region extends from 40°S to 40°N and from 70°E to 180°E.

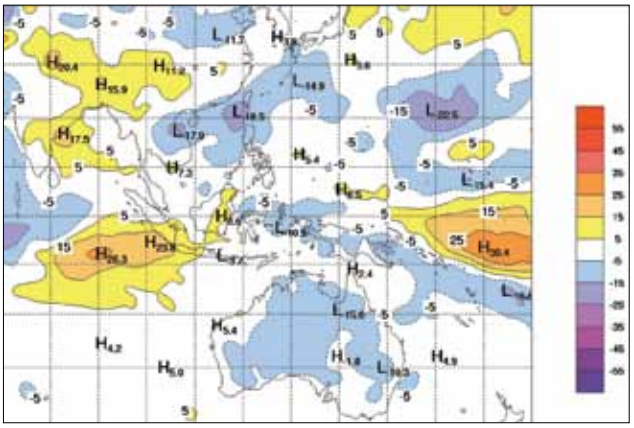

For more information about Australian rainfall patterns during positive and negative IOD years, see Meyers et al. (2007). The weekly IOD values were obtained from Japan Agency for Marine-Earth-Science and Technology (JAMSTEC[7]) and averaged to obtain the monthly IOD values.

During spring 2011, the IOD index was strongly positive in September, with an average monthly value of +0.90 (Fig. 4). During October and November, the positive IOD values slowly reduced to be near neutral values by the end of spring, with monthly values of +0.57 and +0.15 respectively. This follows the moderately positive IOD values recorded during most of winter.

Madden-Julian Oscillation

The Madden-Julian Oscillation (MJO) is a tropical atmospheric anomaly which develops in the Indian Ocean and propagates eastwards into the Pacific Ocean (Zhang, 2005). The MJO takes approximately 30 to 60 days to reach the western Pacific, with a frequency of six to twelve events per year (Donald et al, 2004). When the MJO is in the active phase, it is associated with increased tropical rainfall. A description of the MJO index and the associated phases can be found in Wheeler and Hendon (2004). The phase-space of the MJO index for spring 2011 is shown in Fig. 5 and the evolution of the tropical convection anomalies as represented by OLR (mid-June to mid-December 2011) is shown in Fig. 6.

The MJO was fairly inactive for most of September, until the end of the month, where it became a little more active in the Maritime Continent region in Phase 5 and 6 (Fig. 5). In October, the MJO slowly strengthened as it moved eastwards from the Western Pacific region in to the western hemisphere and Africa (~50°W) in Phases 8 and 1, where it reached record amplitude on 18–19 October. At the end of October,

Fig. 4. Time series of the IOD for the period January 2010 to December 2011. Red values represent positive IOD values and blue values negative IOD values. The dark shades represent values greater than one standard deviation and the crosses are weekly values. The base period is from 1971–2000.

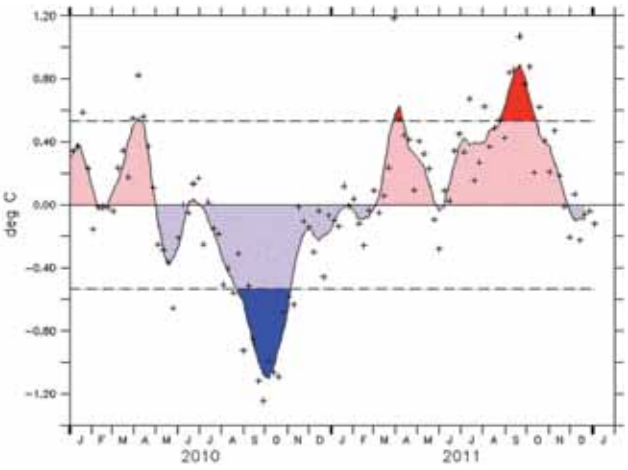

Fig. 5. Phase-space representation of the standardised two-component MJO index (after Wheeler and Hendon, 2004), for the three months from September to November 2011. Each dot represents the value of the index on a particular day, within the eight defined phases of the MJO. Activity in the central circle signifies a weak MJO index. Approximate geographical locations of the MJO for each quadrant are indicated.

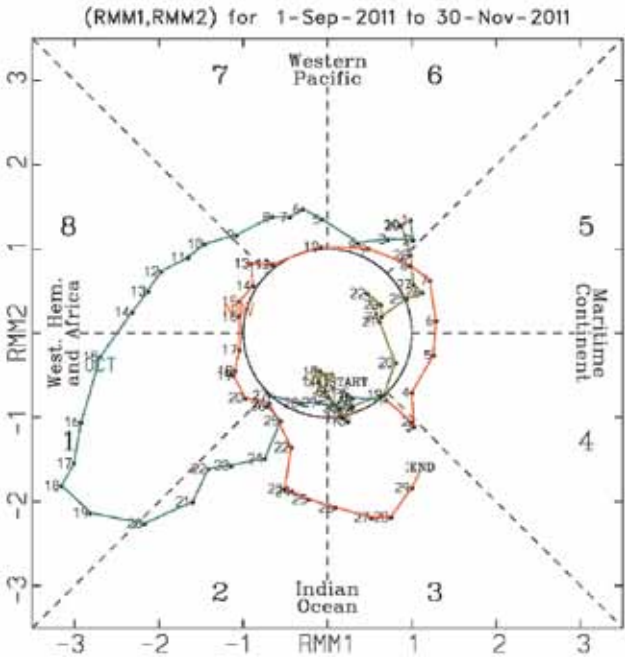

[7]Obtained from http://www.jamstec.go.jp/frcgc/research/d1/iod/DATA/dmi.weekly.ascii.

the MJO weakened as it moved into the central Indian Ocean (Phase 2 and 3). In November, the MJO remained fairly weak in the Maritime Continent region, and then moved eastward, before increasing in amplitude towards the end of the month in the central Indian Ocean (Phases 2 and 3). In Fig. 6, the lower OLR values associated with MJO activity in October in the Atlantic region (~50°W) and in November in the Indian Ocean region (60°E to 100°E) can be seen. The impact of the MJO on Australian rainfall is greatest in austral summer (Phases 4 to 6), but still important in austral spring when the MJO is in Phases 4 to 7 (Wheeler et al, 2009).

Fig. 6. Time-longitude section of daily-averaged OLR anomalies, averaged for 15°S to 15°N, for the period June 2011 through to December 2011. Anomalies are with respect to a base period of 1979–2010.

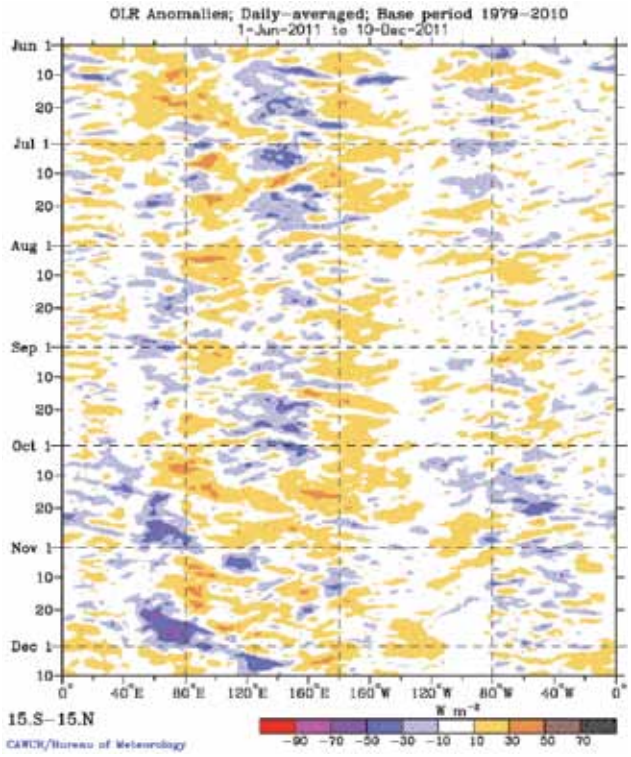

Oceanic patterns

Sea surface temperatures

Global sea surface temperature (SST) anomalies for spring 2011, obtained from the US National Oceanic and Atmospheric Administration (NOAA) Optimum Interpolation analyses (Reynolds et al. 2002), are shown in Fig. 7. The base period is 1961–1990. The negative anomalies (cool SSTs) are shown in blue shades and the positive (warmer SSTs) anomalies in red. Much of the equatorial Pacific east of 170°E is dominated by cooler than average SST anomalies, with the largest values, in the eastern Pacific Ocean, between -1.0° to -1.5 °C. The symmetry of the negative anomalies north and south of the equator indicates an increase in the upwelling along the equator due to stronger easterly trade winds (discussed later under 'Winds') and this pattern is typical of La Niña conditions. In contrast, warmer SSTs were recorded over the northwest Pacific Ocean, parts of the southwest Pacific near Fiji and Tahiti. These warm SST anomalies had initially developed in the middle of last year (Ganter, 2011) due to the strong La Niña, and have persisted for over twelve months. In the Indian Ocean, and adjacent to the south and west of Australia, warmer SST anomalies had also persisted for at least twelve months.

All three of the standard monthly NINO indices (NINO3, 3.4 and 4) cooled significantly during spring, with the largest fall in the NINO3 index. The NINO3 index had values of -0.4 °C, -0.6 °C and -0.8 °C in September, October and November respectively, indicating that the fastest cooling occurred in the tropical eastern Pacific. The NINO3.4 index had a value of -0.6 °C in September, -0.7 °C in October and -0.9 °C in November and the NINO4 index a value of -0.4 °C in September, -0.4 °C in October and -0.5 °C in November. The NINO2 index also showed cooling from September to November, with the index changing from near zero to -0.4 °C respectively. In contrast, the NINO1 index warmed slightly from -0.2 °C in September to -0.1 °C in November.

Fig. 7. Anomalies of SST for spring 2011 (°C).

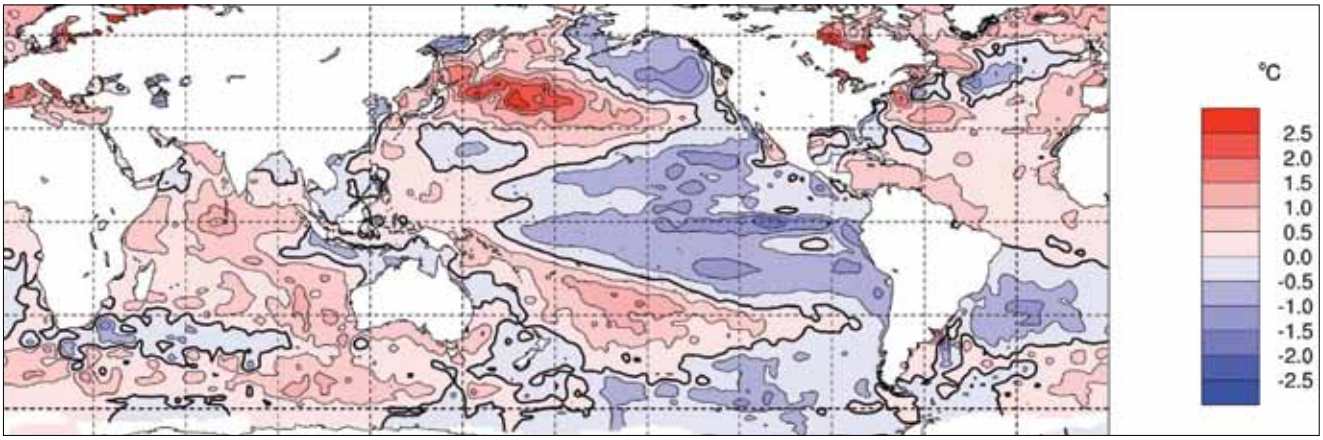

Fig. 8. Time-longitude section of the monthly anomalous depth of the 20 °C isotherm at the equator (2°S to 2°N) for January 2009 to November 2011. (Plot obtained from the TAO Project Office).

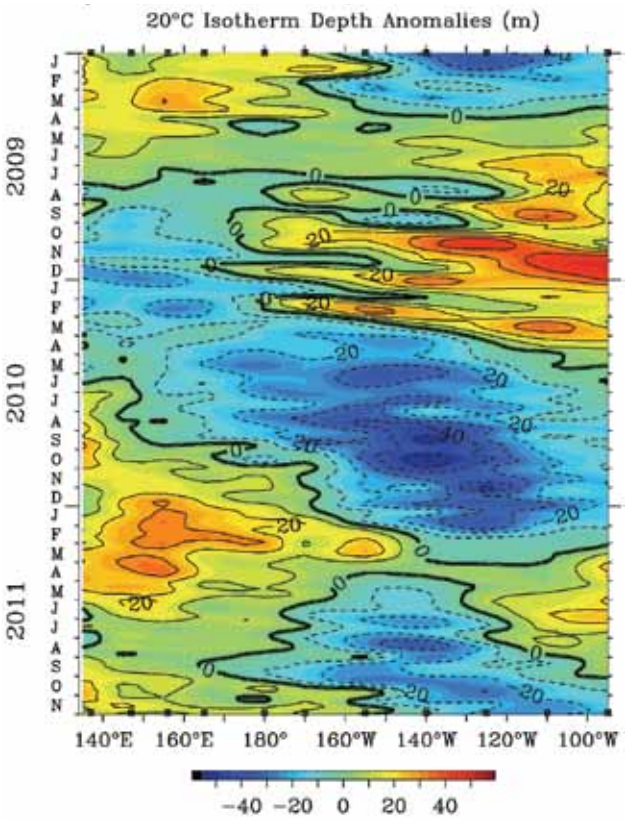

Fig. 9. Four-month August 2011 to November 2011 sequence of subsurface temperature anomalies at the equator for the Pacific Ocean. The contour interval is 0.5 °C. (Plot obtained from CAWCR).

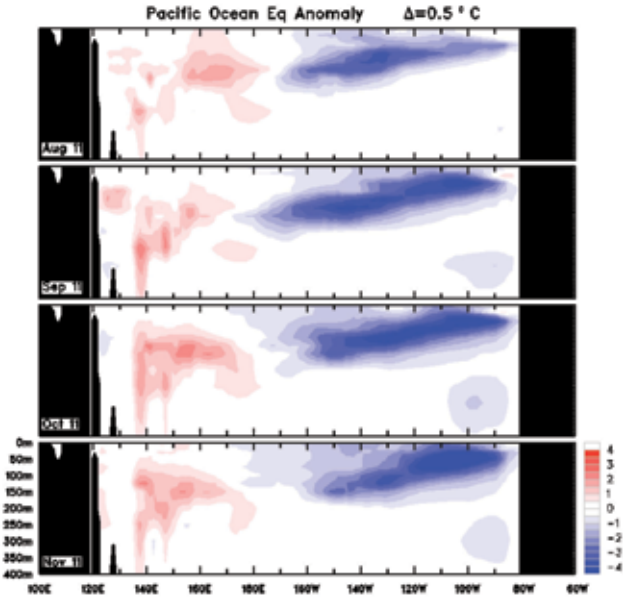

Subsurface patterns

The Hovmöller diagram for the 20 °C isotherm depth anomaly along the equator (2°S to 2°N) from January 2009 to November 2011 (obtained from the NOAA's TAO/TRITON data[8]), is shown in Fig. 8. The 20 °C isotherm is generally located close to the equatorial thermocline, the region of greatest temperature gradient with depth and the boundary between the warm near-surface and cold deep-ocean waters. Therefore, measurements of the 20 °C isotherm depth make a good proxy for the thermocline depth. Positive depth anomalies correspond to the 20 °C isotherm being deeper than average, whereas negative depth anomalies indicate the 20 °C isotherm being more shallow than average. Changes in thermocline depth may act as a precursor to changes at the surface. A shallow thermocline depth results in more cold water available for up-welling, and therefore potential cooling of surface temperatures.

After the major La Niña event during 2010–2011 (where negative cool anomalies dominated the thermocline in the central and eastern equatorial Pacific; Fig. 8), the thermocline returned to near average depths in March–April 2011. However, from April, the thermocline depth again began to decrease over much of the central Pacific, and by August, this negative anomaly had extended westward (west of the International Date Line) and eastward across the equatorial Pacific to exceed -20 m in several regions. By September, the negative thermocline anomaly reached its maximum extent, before retreating into the central and eastern equatorial Pacific region by the end of November.

Figure 9 shows a cross-section of monthly vertical temperature anomaly from August to November 2011, from 120°E to 80°W and to a maximum depth of 400 m across the equatorial Pacific Ocean (obtained from CAWCR). Red shading indicates positive (warm) anomalies, and blue shading indicates negative (cool) anomalies. In July 2011, cool subsurface anomalies had developed in the central and eastern Pacific Ocean and increased markedly in August (Tobin, 2012). By September, the cool anomaly had intensified (maximum > -4 °C) and extended westward to the International Date Line, consistent with the changes in the thermocline described above. By November, the maximum cool anomalies had shifted a little further eastwards and were now located mostly in the central and eastern Pacific. The warm anomaly in the western Pacific near Papua New Guinea persisted for all of spring 2011.

Atmospheric patterns

Surface analyses

The southern hemisphere spring 2011 MSLP pattern, computed from the Bureau of Meteorology's Australian Community Climate and Earth System Simulator[9] (ACCESS)

[8]Hovmöller plot obtained from http://www.pmel.noaa.gov/tao/jsdisplay/

[9]For more information on the Bureau of Meteorology's ACCESS model, see http://www.bom.gov.au/nwp/doc/access/NWPData.shtml.

Fig. 10. Spring 2011 MSLP (hPa). The contour interval is 5 hPa.

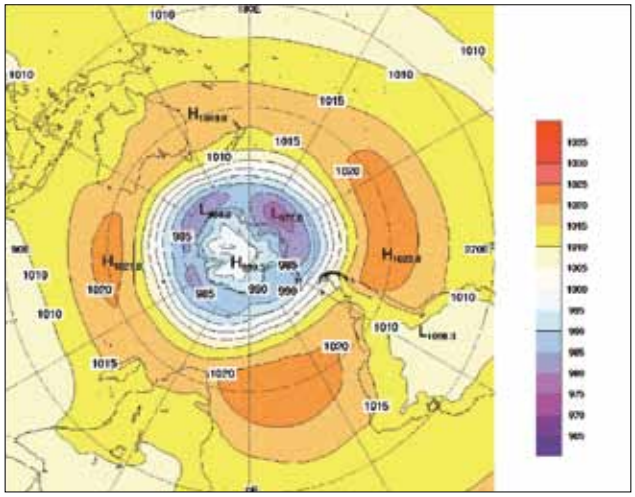

Fig. 11. Spring 2011 MSLP anomalies (hPa), using the 1979–2000 climatology.

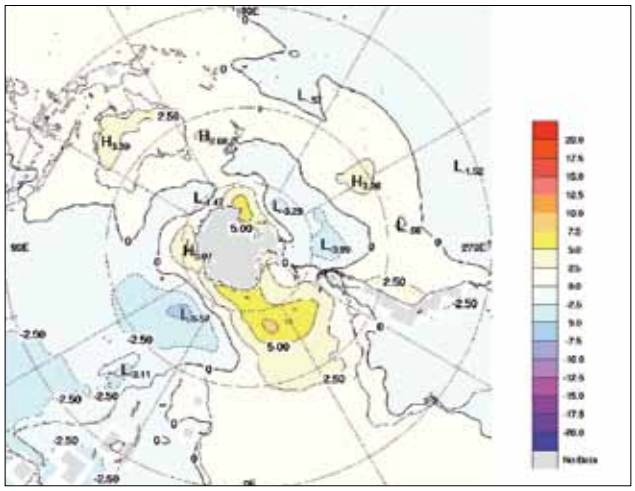

Fig. 12. Spring 2011 500 hPa mean geopotential height (gpm).

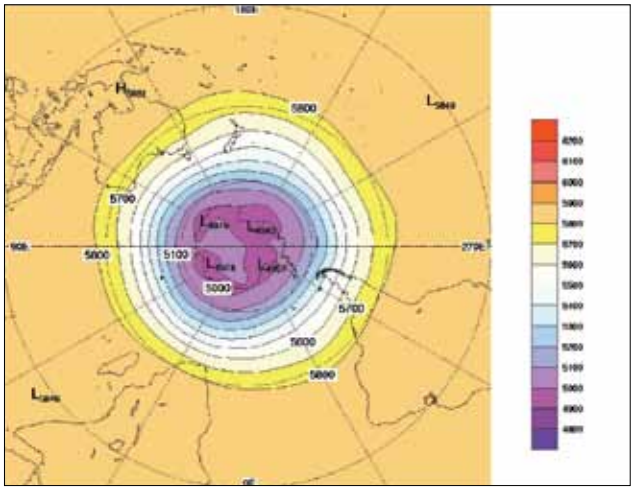

Fig. 13. Spring 2011 500 hPa mean geopotential height anomalies (gpm).

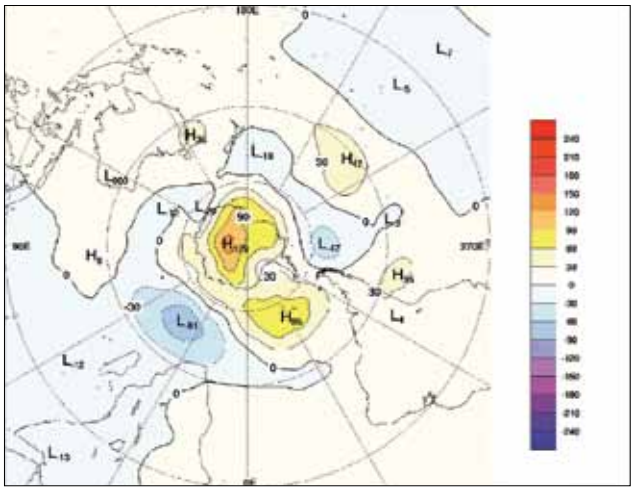

model (the previous GASP model was phased out in August 2010), is shown in Fig. 10. The associated anomaly map pattern is shown in Fig. 11. The MSLP anomalies are the difference from 1979–2000 climatology obtained from the National Centers for Environmental Prediction (NCEP) II Reanalysis data (Kanamitsu et al. 2002). The MSLP analysis has been computed using data from the 0000 UTC daily analyses of the Bureau of Meteorology's Global Assimilation and Prognosis (GASP) model. The MSLP anomaly field is not shown over areas of elevated topography (grey shading).

Figure 10 shows the spring 2011 MSLP pattern was zonal around Antarctica between the latitudes of about 40°S to 60°S. The subtropical ridge formed a band of high pressure around the southern hemisphere centred on 35°S, with centres of high pressure located in the southern Indian Ocean (1021.8 hPa), the eastern Pacific (1023.6 hPa) and the south Atlantic (between 1020 to 1025 hPa). A smaller centre of high pressure was located in the Tasman Sea (1019.0 hPa). The circumpolar low pressure belt is evident around the Antarctic coast at high latitudes (60°-70°S), with the main low centres in the Amundsen Sea (977.6 hPa) and the region north of Wilkes Land (980.8 hPa). The Antarctic high centred near the South Pole had a MSLP of 999.3 hPa. The MSLP was higher in the Australian region for spring 2011, with positive MSLP anomalies of +3.3 hPa and +2.5 hPa over northern Australia (Fig. 11). The highest MSLP positive anomalies were located over the South Atlantic (~330°E), with values as high as +7.5 hPa, and extending south towards the Antarctic coast. Positive MSLP anomalies also occurred over the South Pacific Ocean centred on about 30°S, with a maximum anomaly of +3.1 hPa at 240°E. The largest negative MSLP anomalies occurred in the south Indian Ocean south of Africa (-5.6 hPa) and also near the Amundsen Sea (-4.0 hPa), associated with the circumpolar lows.

Mid-tropospheric analyses

The 500 hPa geopotential height (gpm), which is an indicator of the steering of surface synoptic systems across the southern hemisphere for spring 2011, is shown in Fig. 12. The spring 500 hPa geopotential height field shows the southern

hemisphere mid-high latitudes are dominated by zonal flow, with four weak troughs located the Indian Ocean at ~100°E, the New Zealand region (~170°E), the eastern Pacific Ocean (~80°W) and the Atlantic Ocean (30°W). The lowest 500 hPa geopotential height values are over Antarctica, with the lowest value of 4943 gpm over Marie Byrd Land. The associated 500 hPa geopotential height anomalies (gpm) (Fig. 13) shows the largest positive anomalies are located over the Antarctica (+129 gpm) and the South Atlantic Ocean (+85 gpm). Smaller positive anomalies are located near southeast Australia (+36 gpm) and in the mid-latitudes in the South Pacific Ocean (+47 gpm). Negative anomalies occur in the south Indian Ocean (-81 gpm) southeast of Africa, and to the southwest of South America (-47 gpm).

Southern Annular Mode

The Southern Annular Mode (SAM, also known as the Antarctic Oscillation or AAO) describes the variation of atmospheric pressure between the polar and mid-latitude regions of the southern hemisphere. Positive phases of SAM are characterised by increased mass over the extra-tropics, decreased mass over Antarctica and a poleward contraction of the mid-latitude westerly winds and associated storm tracks. Conversely, negative phases of the SAM indicate decreased mass over the extra-tropics, increased mass over Antarctica and an equatorward expansion of westerly winds and associated storm tracks. A similar oscillation occurs in the northern hemisphere associated with the Northern Annular Mode (also know as the Arctic Oscillation). The Climate Prediction Center[10] produces a daily and monthly AAO index from MSLP observations. In September, the monthly standardised value of the SAM index was -1.25, followed by October (+0.39) and November (-0.91), with a season mean of -0.59. This indicates spring was dominated mainly by negative values in the SAM index, consistent with the MSLP and geopotential height anomalies in Figs. 11 and 13 respectively. The SAM index has been shown to influence Australia temperature patterns (Hendon et al, 2007), as well as rainfall over southwest Western Australia (Cai and Cowan, 2006). A long-term trend towards positive values in the SAM index due to ozone depletion has been noted in previous studies (Thompson and Solomon, 2002).

Blocking

The time-longitude section of the daily southern hemisphere blocking index[11] is shown in Fig. 14. This blocking index (m s^{-1}) is a measure of the strength of the zonal 500 hPa flow in the mid-latitudes (40°S to 50°S), relative to that of the subtropical (25°S to 30°S) and high (55°S to 60°S) latitudes. Positive values of the blocking index are generally associated with a split in the mid-latitude westerly flow near 45°S and mid-latitude blocking activity. Figure 15 shows the mean seasonal index of blocking for each longitude.

Southern hemisphere blocking was below average (Fig. 15) over the Australian and Pacific regions (120°E to 120°W) and above average over the Atlantic Ocean (60°W to 20°E) during spring 2011. The above average blocking over the Atlantic Ocean was also seen in the higher MSLP anomalies in the same region in Fig. 11. Over South Africa and the western Indian Ocean (30°E to 80°E), the blocking index was near average for the whole season with values mostly negative, except for a brief period in mid-late October, when positive values and major blocking occurred (Fig. 14).

Fig. 14. Spring 2011 daily southern hemisphere blocking index (m s^{-1}) time-longitude section. The horizontal axis shows degrees east of the Greenwich meridian. Day one is 1st of September.

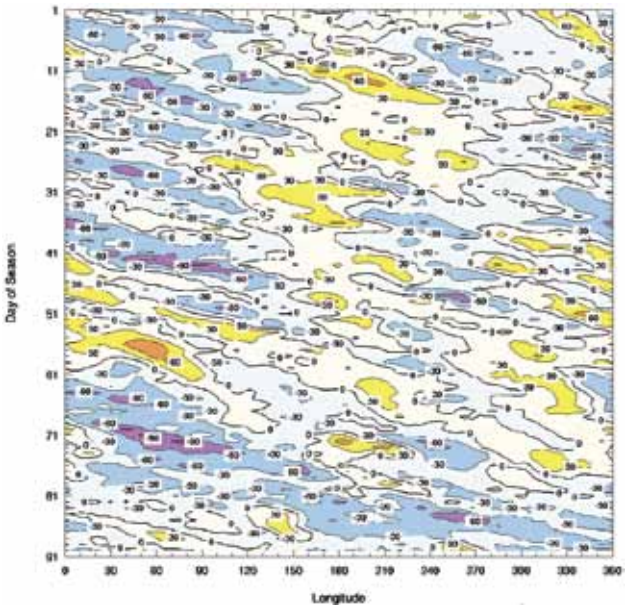

Fig. 15. Mean southern hemisphere blocking index (m s^{-1}) for spring 2011 (solid line). The dashed line shows the corresponding long-term average. The horizontal axis shows degrees east of the Greenwich meridian.

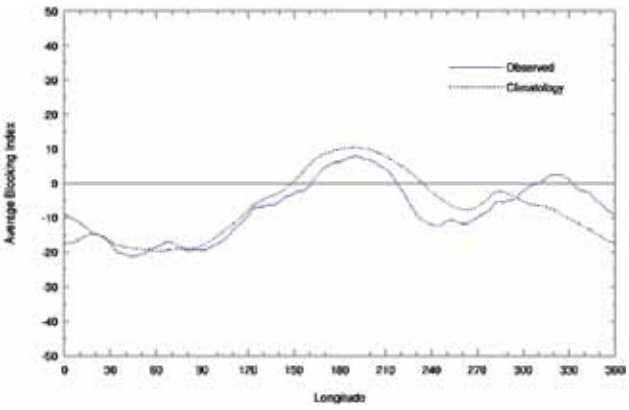

[10]For more information on the SAM index from the Climate Prediction Center (NOAA), see http://www.cpc.ncep.noaa.gov/products/precip/CWlink/daily_ao_index/aao/aao.shtml

[11]The blocking index is defined as $\mathbf{BI} = 0.5\,[(u_{25} + u_{30}) - (u_{40} + 2\,u_{45} + u_{50}) + (u_{55} + u_{60})]$, where u_x is the westerly component of the 500 hPa wind at latitude x.

Winds

Spring low-level (850 hPa) and upper-level (200 hPa) wind anomalies (computed from ACCESS and the twenty-two year NCEP II climatology) are shown in Figs 16 and 17 respectively. Isotach contours are at 5 m s^{-1} intervals. In the low-level winds (Fig. 16), enhanced easterly trade winds dominated the tropical Pacific east of Fiji, a continuation of the stronger trade winds which also occurred in winter (Tobin, 2012), and consistent with developing La Niña conditions. Westerlies south of Australia and Tasmania were slightly stronger than normal. The upper-level (200 hPa) wind anomalies show two main features in the Australia-Pacific region (Fig. 17). Westerly wind anomalies over the equator north of Australia extend into the central Pacific and indicate a strengthened Walker circulation. This typically occurs in La Niña years, with increased convection over the Maritime Continent and the Australian region and increased subsidence over the eastern Pacific. In the South Pacific, stronger westerlies are observed in the mid-latitudes, south of 30°S.

Australian region

Rainfall

Australian spring rainfall totals and rainfall deciles are shown in Figs 18 and 19 respectively. The spring rainfall deciles are calculated with respect to gridded rainfall data from 1900 to 2011. A summary of the seasonal rainfall ranks and extremes are shown in Table 1 for each State and Territory. The percentage areas of rainfall below and above the lowest decile and highest decile respectively, as well as the lowest and highest rainfall on record are shown in Table 2.

Spring rainfall was above average (+57 per cent) over much of Australia and the ninth highest on record, especially in Western Australia, the Northern Territory and parts of South Australia, Queensland and New South Wales. In Western Australia and the Northern Territory, rainfall was the second and sixth highest on record and several areas received their highest rainfall on record (i.e. the western Interior and parts of the Goldfields district in Western Australia and parts of

Fig. 16. Spring 2011 850 hPa vector wind anomalies (m s^{-1}).

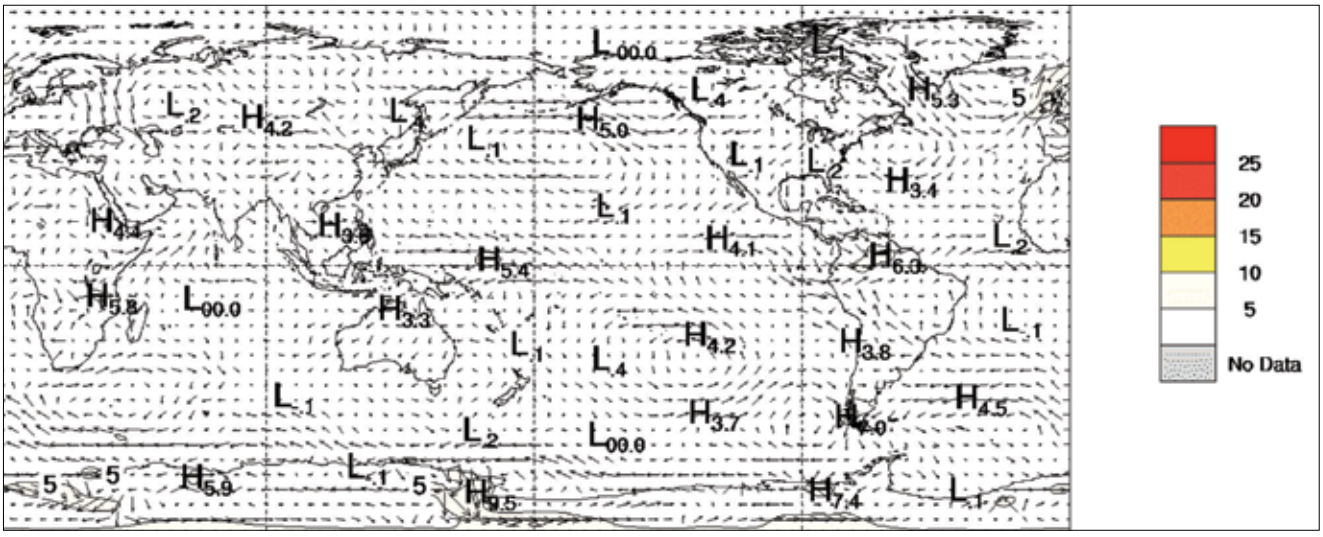

Fig. 17. Spring 2011 200 hPa vector wind anomalies (m s^{-1}).

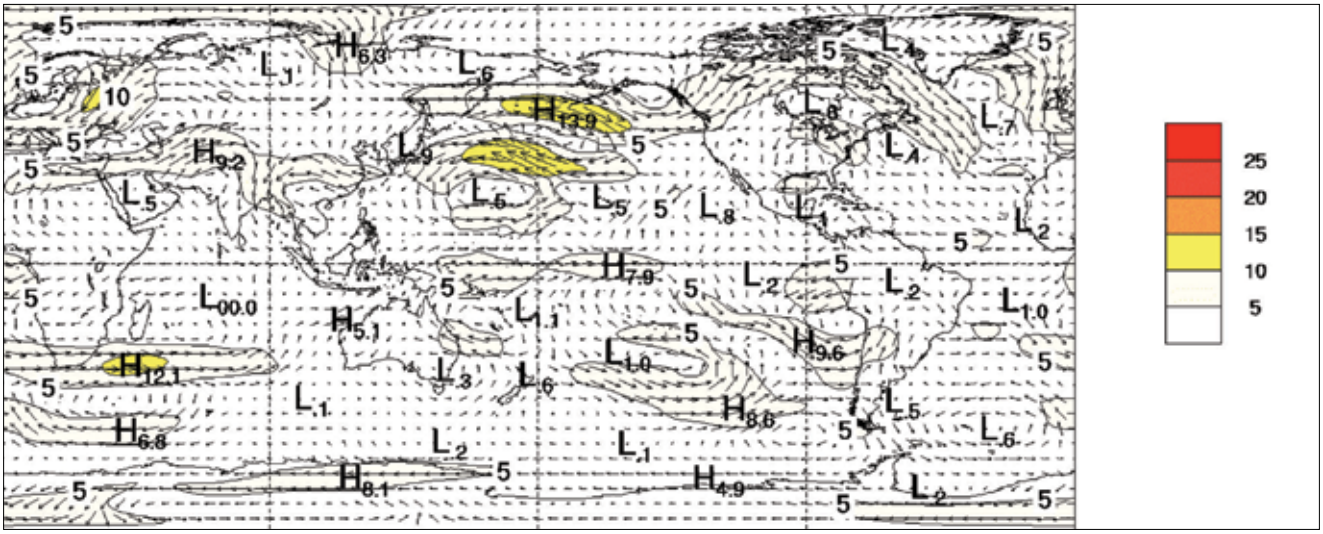

the Roper-McArthur and Barkly districts in the Northern Territory). The highest seasonal rainfall total was recorded at Bellenden Ker Top Station in Queensland with 2453.0 mm. Above average rainfall also occurred over the northern half of the Murray-Darling Basin (regional anomaly +41 per cent), where some areas received their highest rainfall on record (i.e. parts of the North West Slopes and Plains district). In contrast, rainfall was below average or very much below average over coastal Queensland between Brisbane and Townsville, and also in the southwest of Victoria.

Spring rainfall was in the highest decile (wettest ten per cent of all years) for 44.8 per cent by area of Australia, with the highest rainfall on record for 4.04 per cent of Australia (Table 2). Particularly high values of rainfall in the highest decile were recorded in Western Australia (72.3 per cent), the Northern Territory (63.3 per cent), South Australia (30.2 per cent) and New South Wales (25.3 per cent). Western Australia and the Northern Territory also recorded their highest rainfall on record for 9.04 per cent and 4.75 per cent of their State respectively. Only Tasmania did not record any rainfall in the highest decile. On a monthly basis, September was particularly dry in most areas of Australia, but in October and November, rainfall was above average in most regions. A summary of the monthly rainfall highlights from September, October and November is given below.

In September, rainfall over Australia was generally below

Table 1. Summary of the seasonal rainfall ranks and extremes on a national and State basis for spring 2011. The ranking in the second-last column goes from 1 (lowest) to 112 (highest) and is calculated over the years 1900–2011.

Region	*Highest seasonal total (mm)*	*Lowest seasonal total (mm)*	*Highest daily total (mm)*	*Area-averaged rainfall (mm)*	*Rank of area-averaged rainfall*	*% difference from the mean*
Australia	2453.0 at Bellenden Ker Top Station	Zero at several locations	440.0 at Bellenden Ker Top Station, 19 October	114	104	+57
Queensland	2453.0 at Bellenden Ker Top Station	2.6 mm at Coen Airport	440.0 at Bellenden Ker Top Station, 19 October	97	75	+15
New South Wales	719.0 mm at Perisher Valley AWS	47.6 at Broken Hill (Langwell)	190.5 mm at Gwyder River (Gravesend Rd Bdg) Gwydir R, 26 November	183	102	+47
Victoria	657.0 at Mount Baw Baw	59.4 at Murray Lock Number 9	101.0 at Tolmie (Mount Tablet), 29 September	185	65	+2
Tasmania	1170 mm at Mount Read	105.4 mm at Fingal (Legge Street)	110.6 at Eddystone Point, 27 November	365	57	0
South Australia	214.3 at Piccadilly (Woodhouse)	1.0 at Muloorina Station (Muloorina Homestead)	56.0 at Cameron Corner (Lind), 22 November	72	91	+42
Western Australia	390.8 at Vermeulen	Zero at several locations	83.0 at The Oaks, 23 October	95	111	+131
Northern Territory	442.8 at Geriatric Park	0.0 at Anningie	137.0 at Daly Waters, 20 November	135	107	+100

Table 2. Percentage areas in different categories for spring 2011 rainfall. 'Severe deficiency' denotes rainfall at or below the 5th percentile. Areas in decile 1 include those in 'severe deficiency', which in turn include those which are 'lowest on record'. Areas in decile 10 include those which are 'highest on record' Percentage areas of highest and lowest on record are given to two decimal places because of the small quantities involved; other percentage areas to one decimal place.

Region	*Lowest on record*	*Severe deficiency*	*Decile 1*	*Decile 10*	*Highest on record*
Australia	0.00	0.3	1.0	44.8	4.04
Queensland	0.00	1.1	4.1	15.9	0.49
New South Wales	0.00	0.0	0.0	25.3	1.48
Victoria	0.00	0.0	0.0	2.6	0.00
Tasmania	0.00	0.0	0.0	0.0	0.00
South Australia	0.00	0.0	0.0	30.2	0.00
Western Australia	0.00	0.0	0.1	72.3	9.04
Northern Territory	0.00	0.2	0.2	63.3	4.75

average (-24 per cent), and this included most of the Northern Territory, South Australia, Queensland and Victoria, a continuation of the dry conditions from winter (Tobin, 2012). Very much below average rainfall was recorded in eastern and central parts of Western Australia, parts of eastern central Queensland, northern, central and eastern parts of South Australia and the adjacent regions in western Victoria and southwest New South Wales. However, only a few small regions in southeast South Australia and adjacent areas in New South Wales and Victoria had the lowest rainfall on record. In contrast, rainfall was very much above average in southwest Queensland and northern New South Wales and a small region in the Goldfields of Western Australia. Most of the rainfall in New South Wales, southern Queensland and central and eastern Victoria occurred on 28–29 September.

In October, rainfall was above average (+64 per cent) over Australia and very much above average in Western Australia, western and northern regions of the Northern Territory, northern Queensland and parts of southeast Queensland. Western Australia recorded its third highest rainfall (+219 per cent) for October. Very much below average rainfall occurred in a few small regions in southwest Queensland and the adjacent Northern Territory. Major rainfall was recorded in southeast Queensland on 13–17 October. From 18–31 October, a series of cold fronts and troughs produced widespread showers and thunderstorms across Western Australia, the Northern Territory and South Australia, before moving further eastward. On 22 October, particularly severe thunderstorms were reported from the Goldfields in Western Australia. Severe thunderstorms also occurred on 28 October in Victoria and in Melbourne, with widespread rainfall, and golf ball size hail was reported from Mildura.

In November, rainfall was again above average (+93 per cent) over Australia and the fourth highest on record. Every State or Territory received above average rainfall. Very much above average rainfall occurred over the Northern Territory, Western Australia, northern South Australia, much of New South Wales and Victoria and the north coast of Tasmania. Rainfall in Western Australia and the Northern Territory was the second and fourth highest on record respectively, a prelude to above average rainfall over Western Australia during the 2011–2012 wet season. In contrast, rainfall over coastal eastern Queensland between Brisbane and Townsville was very much below average, with some areas receiving their lowest rainfall on record. In the first week of November, rainfall continued over much of Western Australia, parts of the Northern Territory and the adjacent western parts of Queensland due to a slow moving inland heat trough, with a deep moist northerly flow over Western Australia. In the second week, heavy rainfall was recorded in Victoria and southern New South Wales and also parts of the Northern Territory and the Kimberley in Western Australia due to slow moving heat troughs and moist conditions. On 9 November, particularly severe thunderstorms over eastern South Australia, Victoria and western parts New South Wales produced widespread rainfall with some heavy falls. In the third week, heavy rainfall was recorded over nearly all of the Northern Territory and adjacent parts of Queensland and much of New South Wales. Heavy rainfall continued up to the end of the month over much of the Northern Territory, Queensland, New South Wales and Victoria, due to a slow moving low which formed in the east coast trough. The heaviest rainfall (> 200 mm) occurred in northern New South Wales, with some flooding on the Namoi, Gwydir and Dumaresq/Severn rivers.

Drought

During spring 2011, most of Australia received above average rainfall and this eased the below average rainfall experienced in many regions of Australia during the winter months, especially over the Murray-Darling Basin, Victoria and parts of southern Western Australia (Tobin, 2012). However, in coastal parts of eastern Queensland, rainfall was very much below average during spring. A way the Bureau of Meteorology currently assesses drought is by considering the extent of areas of the country which contain accumulated rainfall in the lowest deciles for varying timescales. To the end of November 2011, 0.3 per cent of Australia was in 'severe deficiency', with 1.1 per cent of Queensland and 0.1 per cent of the Northern Territory by area (Table 2). No regions in Australia recorded the lowest rainfall for spring 2011. This was an improvement from the end of winter, where 0.4 per cent of Australia was considered in 'severe deficiency' (Tobin, 2012). A summary of the rainfall area below decile one and the lowest rainfall on record is shown in Table 2 for each State and Territory.

Temperature

Figures 20 and 21 show the maximum and minimum temperature anomalies respectively for spring 2011. The anomalies have been calculated with respect to the 1961–1990 period, and use all stations for which an elevation is available. Station normals have been estimated using gridded climatologies for those stations with insufficient data within the 1961–1990 period to calculate a station normal directly. Figures 22 and 23 show spring maximum and minimum temperature deciles respectively, calculated using monthly temperature analyses from 1911 to 2011. A summary of the maximum and minimum temperature deciles for each State and nationally is shown in Table 3, with ranks and extremes in Tables 4 and 5.

Maximum temperatures averaged over Australia were warmer (+0.31 °C) than average for spring 2011, with the largest positive anomalies recorded in Victoria (+1.46 °C) and Tasmania (+1.24 °C), followed by New South Wales (+1.14 °C), South Australia (+1.11 °C) and Queensland (+0.54 °C). The highest daily maximum temperature was recorded at Birdsville Airport in November, with 44.1 °C. The maximum temperature anomalies in Tasmania and Victoria were the second and seventh warmest on record, respectively. The mean temperature anomaly for Victoria and Tasmania was (+1.25 °C) and (+0.83 °C) respectively, the third and fourth

Fig. 18. Spring 2011 rainfall totals (mm) for Australia.

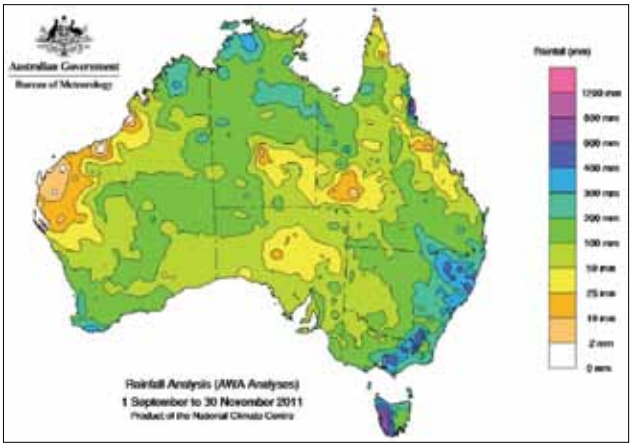

Fig. 19. Spring 2011 rainfall deciles for Australia: decile ranges based on grid-point values over the spring 1900–2011.

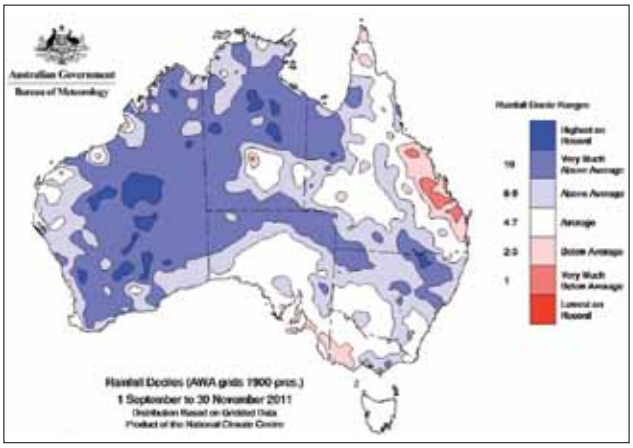

Fig. 20. Spring 2011 maximum temperature anomalies (°C).

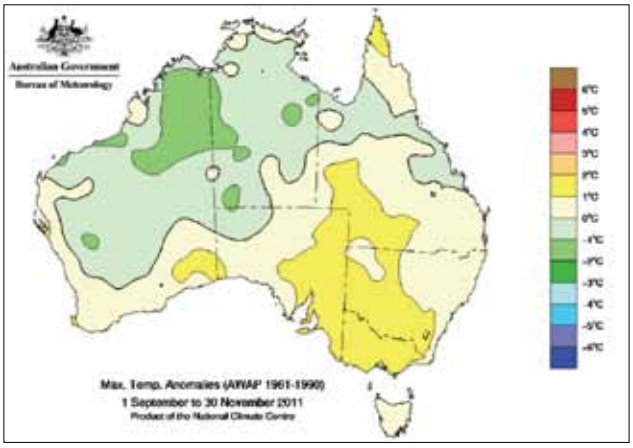

Fig. 21. Spring 2011 minimum temperature anomalies (°C).

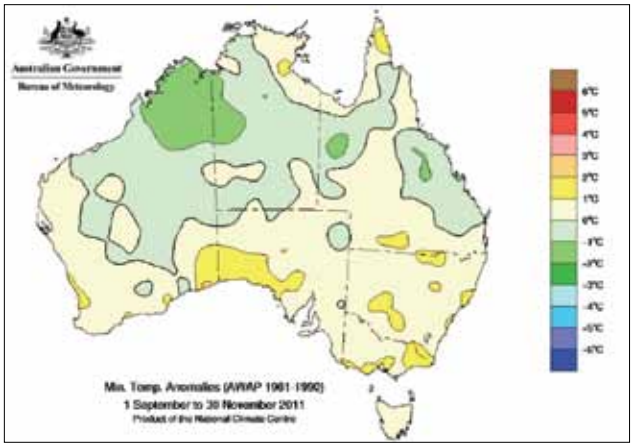

Fig. 22. Spring 2011 maximum temperature deciles: decile ranges based on grid-point values over the spring 1911–2011.

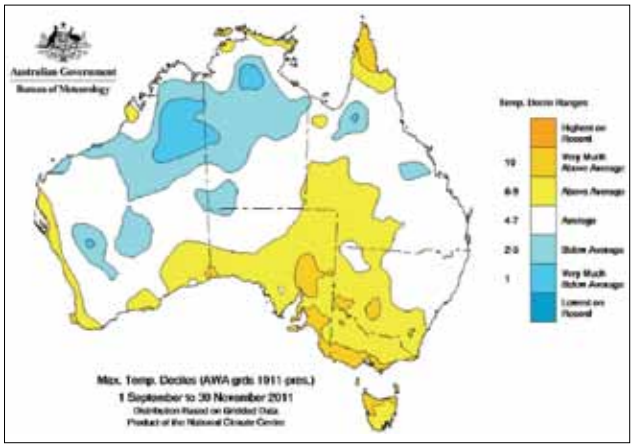

Fig. 23. Spring 2011 minimum temperature deciles: decile ranges based on grid-point values over the spring 1911–2011.

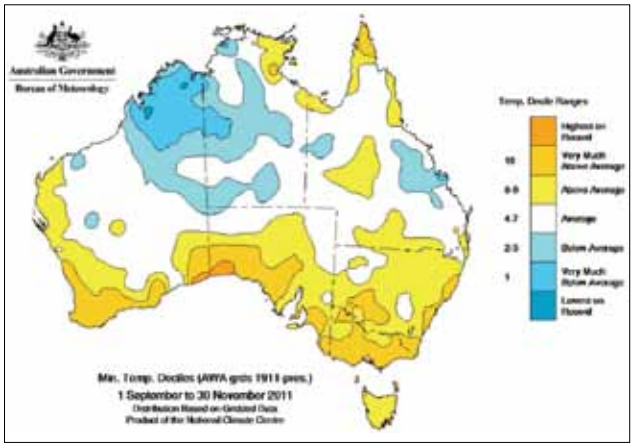

Table 3. Percentage areas in different categories for spring 2011. Areas in decile 1 include those which are 'lowest on record'. Areas in decile 10 include those which are 'highest on record'. Percentage areas of highest and lowest on record are given to two decimal places because of the small quantities involved; other percentage areas to one decimal place. Gridpoint deciles calculated with respect to 1911–2011.

Region	*Maximum temperature*				*Minimum temperature*			
	Lowest on record	*Decile 1*	*Decile 10*	*Highest on record*	*Lowest on record*	*Decile 1*	*Decile 10*	*Highest on record*
Australia	0.00	4.0	3.5	0.00	0.17	5.4	10.9	0.46
Queensland	0.00	0.3	3.0	0.00	0.00	0.4	1.7	0.00
New South Wales	0.00	0.0	2.8	0.00	0.00	0.0	14.4	0.00
Victoria	0.00	0.0	23.4	0.00	0.00	0.0	69.5	0.00
Tasmania	0.00	0.0	27.3	0.00	0.00	0.0	1.8	0.00
South Australia	0.00	0.0	10.9	0.00	0.00	0.0	27.1	2.61
Western Australia	0.00	9.1	0.5	0.00	0.53	13.5	10.1	0.37
Northern Territory	0.00	5.7	0.2	0.00	0.00	5.5	0.6	0.00

Table 4. Summary of the seasonal maximum temperature ranks and extremes on a national and State basis for spring 2011. The ranking in the last column goes from 1 (lowest) to 62 (highest) and is calculated over the years 1950–2011[12].

Region	*Highest seasonal mean maximum (°C)*	*Lowest seasonal mean maximum (°C)*	*Highest daily temperature (°C)*	*Lowest daily maximum temperature (°C)*	*Area-averaged temperature anomaly (°C)*	*Rank of area-averaged temperature anomaly*
Australia	37.7 at Wyndham Aero	7.6 at Mount Hotham	44.1 at Birdsville, 15 and 29 November	-3.5 at Mount Hotham, 9 September	+0.31	33
Queensland	35.8 at Century Mine and Julia Creek	21.6 at Applethorpe	44.1 at Birdsville, 15 and 29 November	10.0 at Applethorpe, 10 September	+0.54	42
New South Wales	29.4 at Wanaaring	8.1 at Thredbo AWS	42.2 at Walgett, 15 November	-2.8 at Thredbo, 9 September	+1.14	46
Victoria	25.7 at Mildura	7.6 at Mount Hotham	39.0 at Walpeup, 18 November	-3.5 at Mount Hotham, 9 September	+1.46	56
Tasmania	18.5 at Bushy Park, Friendly Beaches and Launceston (Ti Tree Bend)	8.1 at Mount Wellington	31.0 at Swansea, 6 November	-1.1 at Mount Wellington, 11 September	+1.24	61
South Australia	31.3 at Moomba	17.2 at Mount Lofty	43.4 at Oodnadatta, 29 November	7.9 at Mount Lofty, 10 September	+1.11	51
Western Australia	37.7 at Wyndham Aero	19.2 at Shannon and Albany	44.0 at Wyndham Aero, 12 October and at Roebourne, 13 November	11.0 at Mount Barker, 27 September	-0.20	23
Northern Territory	37.6 at Bradshaw	29.6 at Kulgera	43.6 at Timber Creek, 12 October	14.7 at Kulgera, 21 November	-0.41	18

[12]A high-quality subset of the temperature network is used to calculate the spatial averages and rankings shown in Table 4 (maximum temperature) and Table 5 (minimum temperature). These averages are available from 1950 to the present. As the anomaly averages in the tables are only retained to two decimal places, tied rankings are possible.

Table 5. Summary of the seasonal minimum temperature ranks and extremes on a national and State basis for spring 2011. The ranking in the last column goes from 1 (lowest) to 62 (highest) and is calculated over the years 1950–2011.

Region	*Highest seasonal mean minimum (°C)*	*Lowest seasonal mean minimum (°C)*	*Highest daily minimum temperature (°C)*	*Lowest daily temperature (°C)*	*Area-averaged temperature anomaly (°C)*	*Rank of area-averaged temperature anomaly*
Australia	25.9 at Cape Don	0.8 at Mount Wellington	29.6 at Birdsville, 8 November	-8.9 at Perisher Valley, 8 September	+0.12	32
Queensland	25.0 at Horn Island	8.7 at Applethorpe	29.6 at Birdsville, 8 November	-1.5 at Stanthorpe, 14 September	+0.15	31.5
New South Wales	16.8 at Cape Byron	1.0 at Thredbo	27.2 at Tibooburra, 16 November	-8.9 at Perisher Valley, 8 September	+0.75	47
Victoria	12.2 at Gabo Island	1.4 at Mount Hotham	23.5 at Mildura, 19 November	-7.9 at Mount Hotham, 12 September	+1.03	60
Tasmania	10.8 at Hogan Island	0.8 at Mount Wellington	18.0 at Friendly Beaches, 20 October	-6.0 at Liawenee, 3 October	+0.43	51
South Australia	15.9 at Oodnadatta	6.9 at Keith (Munkora)	27.8 at Oodnadatta, 19 November	-3.6 at Yongala, 7 September	+1.01	53
Western Australia	25.6 at Troughton Island	7.6 at Newdegate	29.2 Troughton Island, 30 November	-4.1 at Eyre, 24 September	-0.12	24.5
Northern Territory	25.9 at Cape Don	12.7 at Arltunga	29.1 at Dum In Mirrie, 29 November	-0.5 at Arltunga, 15 September	-0.71	10

highest on record. Western Australia and the Northern Territory recorded below average maximum temperatures, with -0.20 °C and -0.41 °C anomalies respectively and this was most likely due to above average rainfall. A summary of maximum temperatures ranks and extremes on a national and State basis is shown in Table 4.

Minimum temperatures averaged over Australia were slightly above average (+0.12 °C) for spring 2011, with the largest positive anomalies recorded in Victoria (+1.03 °C), South Australia (+1.01 °C), New South Wales (+0.75 °C), Tasmania (+0.43 °C) and Queensland (+0.15 °C). The lowest daily minimum temperature was recorded at Perisher Valley in September, with -8.9 °C. The minimum temperature anomalies in Victoria and South Australia were the third and tenth warmest on record, respectively. The Northern Territory and Western Australia recorded below average minimum temperatures, with -0.71 °C and -0.12 °C respectively. The minimum temperature anomalies in the Northern Territory were the tenth coolest on record. A summary of minimum temperatures ranks and extremes on a national and State basis is shown in Table 5.

The maximum temperature deciles over Australia are shown in Fig. 22 and are summarised in Table 3. These show a similar pattern to the maximum temperatures shown in Fig. 20. Australia recorded 3.5 per cent of maximum temperatures in the highest decile, with Tasmania, Victoria and South Australia recording 27.3 per cent, 23.4 per cent and 10.9 per cent respectively. No States or Territories had new maximum temperature records. Australia also recorded 4.0 per cent of maximum temperatures in the lowest decile, with Western Australia and the Northern Territory recording 9.1 per cent and 5.7 per cent respectively, but no new records were set.

The minimum temperature deciles over Australia are shown in Fig. 23 and are summarised in Table 3. These show a similar pattern to the maximum temperatures shown in Fig. 21 and are also similar to the maximum temperature patterns. Australia recorded 10.9 per cent of minimum temperatures in the highest decile, with 0.46 per cent a new record. Victoria, South Australia and New South Wales recorded minimum temperatures in the upper decile with 69.5 per cent, 27.1 per cent and 14.4 per cent respectively. South Australia and Western Australia set new records for 2.61 per cent and 0.37 per cent of their State respectively. Australia also recorded 5.4 per cent of minimum temperatures in the lowest decile (0.17 per cent lowest on record), with Western Australia and the Northern Territory recording 13.5 per cent and 5.5 per cent respectively, and 0.53 per cent of Western Australia a new record low.

References

Cai, W. and Cowan, T. 2006. SAM and regional rainfall in IPCC AR4 models: Can anthropogenic forcing account for the southwest Western Australian winter rainfall reduction? *Geophys. Res. Lett., 33*. L24708, doi:10.1029/2006GL028037.

Donald, A., Meinke, H., Power, B., Wheeler, M. and Ribbe, J. 2004. Forecasting with the Madden-Julian Oscillation and the applications for risk management. In: *4th International Crop Science Congress*, 26 September–01 October 2004, Brisbane, Australia.

Ganter, C. 2011. Seasonal climate summary southern hemisphere (winter 2010): A fast developing La Niña. *Aust. Met. Oceanogr. J., 61*, 125–35.

Hendon, H.H., Thompson, D.W.J., and Wheeler, M.C. 2007. Australian rainfall and surface temperature variations associated with the Southern Annular Mode. *J. Clim., 20*, 2452–67.

Imielska, A. 2011. Seasonal climate summary southern hemisphere (summer 2010–2011): second wettest Australian summer on record and one of the strongest La Niña events on record. *Aust. Met. Oceanogr. J., 61*, 241–51.

Kanamitsu, M., Ebisuzaki, W., Woollen, J., Yang, S.-K,, Hnilo, J.J., Fiorino, M. and Potter, G.L. 2002. NCEP-DOE AMIP-II Reanalysis (R-2). *Bull. Am. Meteorol. Soc., 83*, 1631-43.

Kuleshov, Y., Qi, L., Fawcett, R. and Jones, D. 2009. Improving preparedness to natural hazards: Tropical cyclone prediction for the Southern Hemisphere. In: Gan, J. (Ed.), *Advances in Geosciences*, Vol. 12 *Ocean Science*, World Scientific Publishing, Singapore, 127–43.

Lovitt, C. 2011. Seasonal climate summary southern hemisphere (spring 2010): La Niña strengthens. *Aust. Met. Oceanogr. J., 61*, 185–95.

Meyers, G., McIntosh, P., Pigot, L. and Pook, M. 2007. The Years of El Niño, La Niña, and Interactions with the Tropical Indian Ocean. *J. Clim., 20*, 2872–80.

Reynolds, R.W., Rayner, N.A., Smith, T.M., Stokes, D.C. and Wang, W. 2002. An improved in situ and satellite SST analysis for climate. *J. Clim., 15*, 1609-25.

Saji, N.H., Goswami, B.N., Vinayachandran, P.N. and Yamagata T. 1999: A dipole mode in the tropical Indian Ocean, *Nature, 401*, 360-63.

Thompson, D.W.J. and Solomon, S. 2002. Interpretation of recent Southern Hemisphere climate change. *Science, 296*, 895-99.

Tobin, S. 2012. Seasonal climate summary southern hemisphere (winter 2011): A dry season in the lull between La Niña events. *Aust. Met. Oceanogr. J., 62*, in press.

Troup, A.J. 1965. The Southern Oscillation. *Q. J. R. Meteorol. Soc., 91*, 490-506.

Wheeler, M.C. and Hendon, H.H. 2004. An All-Season Real-Time Multivariate MJO Index: Development of an Index for Monitoring and Prediction. *Mon. Weather. Rev., 132*, 1917–32.

Wheeler, M.C., Hendon, H.H., Cleland, S., Meinke, H. and Donald, A. 2009. Impacts of the Madden-Julian Oscillation on Australian Rainfall and Circulation. *J. Clim., 22*, 1482–98.

Wolter, K. and Timlin, M.S. 1993. Monitoring ENSO in COADS with a seasonally adjusted principal component index. Proc. Of the 17th Climate Diagnostics Workshop, Norman, OK, NOAA/NMC/CAC, NSSL, Oklahoma Clim. Survey, CIMMS and the School of Meteorology, Univ. of Oklahoma, 52-7.

Wolter, K. and Timlin, M.S. 1998. Measuring the strength of ENSO – how does 1997/98 rank? *Weather, 53*, 315-24.

Zhang. C. 2005. Madden-Julian Oscillation. *Rev. Geophys., 43*, RG2003, doi:10.1029/2004RG000158.